

Corotation-bounce resonance of ions in Jupiter's magnetosphere

Y. Sarkango¹, J. R. Szalay¹, P. A. Damiano², A. H. Sulaiman³, P. A. Delamere², J. Saur⁴, D. J. McComas¹, R. W. Ebert^{5,6}, F. Allegrini^{5,6}

¹Department of Astrophysical Sciences, Princeton University, USA

²Geophysical Institute, University of Alaska Fairbanks, USA

³School of Physics and Astronomy, University of Minnesota, USA

⁴Institut für Geophysik und Meteorologie, Universität zu Köln, Germany

⁵Southwest Research Institute, USA

⁶Department of Physics and Astronomy, University of Texas at San Antonio, USA

Corresponding author: Yash Sarkango (sarkango@princeton.edu)

Key Points:

- Banded energy distributions (0.01-45 keV/q) occur simultaneously for different ion species mapping to M=10-20.
- Bounce frequencies of banded ions match harmonics of the corotation/System-III frequency.
- Corotation-modulated bounce resonance accelerates low-energy plasma ions in Jupiter's magnetosphere.

Abstract

Banded energy distributions of H^+ , O^{++} , S^{+++} , and O^+ or S^{++} ions between 100 eV to ~20 keV are consistently observed in Jupiter's magnetosphere mapping to M-shells between M=10-20. The bands correspond to flux enhancements at similar speeds for different ion species, providing the first evidence of simultaneous bounce-resonant acceleration of multiple ion species in Jupiter's magnetosphere. Ion enhancements occur for energies at which the bounce frequencies of the trapped ions matched integer harmonics of the System-III corotation frequency. The observations highlight a previously unknown interaction between corotation and bounce motion of <10 keV energy ions that is a fundamental and persistent process occurring in Jupiter's magnetosphere.

Plain Language Summary

Trapped plasma particles in Jupiter's magnetosphere experience a "bounce" motion - traveling from the northern to the southern hemisphere and back along magnetic field lines. In addition, plasma as a whole is driven to rotate with the planet, a process referred to as corotation. These are two distinct periodic processes – the former dictates how individual particles travel along a field line, whereas the latter is a global scale process in the magnetosphere. However, for low energy plasma particles (<10 keV), both processes have similar timescales (>100 min). In this work, we show evidence from plasma measurements of resonance between these two processes, which could also be important for plasma acceleration.

1 Introduction

Particle flux enhancements at discrete energies, which we refer to as "banded energy distributions," have been observed in ion populations throughout the solar system and have been explained by different processes for the energetic and the thermal populations.

1.1. "Zebra-stripes" for energetic particles (> 200 keV electrons and ions)

Energy distributions that appear as zebra-stripes (bands or alternating enhancement and depletions) have been observed for energetic electrons between 40-400 keV and energetic ions at >0.4-1 MeV energies in the magnetospheres of Earth (Lejosne et al., 2022; Lejosne & Mozer, 2020; Pandya et al., 2023, 2024; Sauvaud et al., 2013; Ukhorskiy et al., 2014; Wang et al., 2024), Saturn (Hao et al., 2020; Sun et al., 2021, 2022), and Jupiter (Hao et al., 2020). The physical origins of the zebra-stripe distributions are still under debate. Simulations have reproduced "zebra-stripes" either by using an explicit time-varying electric field (Ukhorskiy et al., 2014), by the influence of a convection electric field (Pandya et al., 2023), by a noon-midnight electric field in the case of Saturn (Sun et al., 2021), or by a dawn-dusk electric field at Jupiter (Hao et al., 2020), without requiring any explicit time-variability in the non-rotating frame. Both at Jupiter and Saturn, a corotation-drift resonance (CDR) mechanism was also proposed in which MeV-energy electrons are quasi-stationary in local time due to gradient-curvature drifts opposing corotation, making them susceptible to other large-scale electric fields (Roussos et al., 2018). Zebra-stripe distributions for energetic particles are not the focus of the present work, we mention them only to avoid confusion.

1.2. Banded energy distributions for low-energy particles (<10 keV electrons and ions)

Banded energy distributions have also been reported for lower energy plasma ions, for which the gradient-curvature drift is negligibly slow, and these are likely produced by a different

process. In Saturn’s magnetosphere, energy-banded ion distributions in the magnetodisc were observed by *Cassini* between M-shells of $M=5.5-6.9$ at 10-200 eV/q energies (Thomsen et al. 2017). Bounce resonance of the particles with standing Alfvén waves in the magnetosphere was proposed to be the explanation for the organized banding.

At Jupiter, banded protons and electrons were discovered in a narrow range of magnetic flux tubes connected to the wakes of the Galilean moons, at energies ranging from 0.2-5 keV (Sarkango et al., 2024). These moon-related flux enhancements were linked to bounce-resonance with standing Alfvén waves in the moons’ wakes. At Jupiter, bounce frequencies for 0.1-1 keV ions are in the mHz range, which is comparable to eigenfrequencies of field-line resonances or standing Alfvén waves in the magnetosphere (Lysak & Song, 2020; Manners et al., 2018; Manners & Masters, 2019). Hence, bounce-resonance between these lower energy ions and field-line resonances was feasible. It was also shown by Sarkango et al., (2024) that the “bands” were equally spaced in speed, not energy, which was consistent with bounce-resonance since bounce frequencies would have been directly proportional to the particles’ speeds.

This manuscript reports on banded energy distributions observed in Jupiter’s magnetosphere by the JADE instrument onboard the *Juno* spacecraft at typical energies <10 keV, mapping to M-shells between 10-20. These observations are unrelated to “zebra-stripe” distributions seen for the energetic particles. In Section 2 we show the relevant observations of banded energy distributions. In Section 3, we discuss the interpretation and significance of the observations and summarize our findings in Section 4.

2 Observations

We used data collected by the Jovian Auroral Distributions Experiment ion sensor (JADE-I) onboard *Juno* near the polar regions of Jupiter (McComas et al. 2017). *Juno* orbits Jupiter in a highly elliptical trajectory and transits across a range of M-shells while in this region near perijove. During this time, JADE-I measured ion fluxes between energies of ~0.01-46 keV/q and mass-per-charge (m/q) of 1 to 64 using an electrostatic analyzer and a time-of-flight (TOF) section. The TOF data is usually averaged to longer cadence of at least one *Juno* spin period of ~30 s and therefore does not contain directional information about the incoming ions.

Juno has encountered numerous intervals near perijove in which banded energy distributions were present in different ion species (identified in m/q vs. energy space) as measured by JADE, often simultaneously. We manually identified periods in the JADE-I data which exhibited multiple bands up to and including *Juno*’s 63rd orbit (see Supporting Information for a list). In Figure 1a, we show the locations of the identified ion banding events in a magnetic coordinate system aligned with a dipole magnetic field, including the CON2020 current sheet (Connerney et al., 2020), to illustrate where these events map to in the magnetodisc. The dipole approximation allows us to compare the magnetic latitude of each event and condense events across longitude, which would otherwise not be possible if using a non-axisymmetric field. Figure 1b-1d shows an example of ion banding during *Juno*’s 61st orbit. In contrast to the banded distributions associated with the Galilean moons (Sarkango et al., 2024) that are shown in red, these new observations (purple) map to M-shells > 10 R_J and were observed at higher altitudes ($h > 0.5 R_J$).

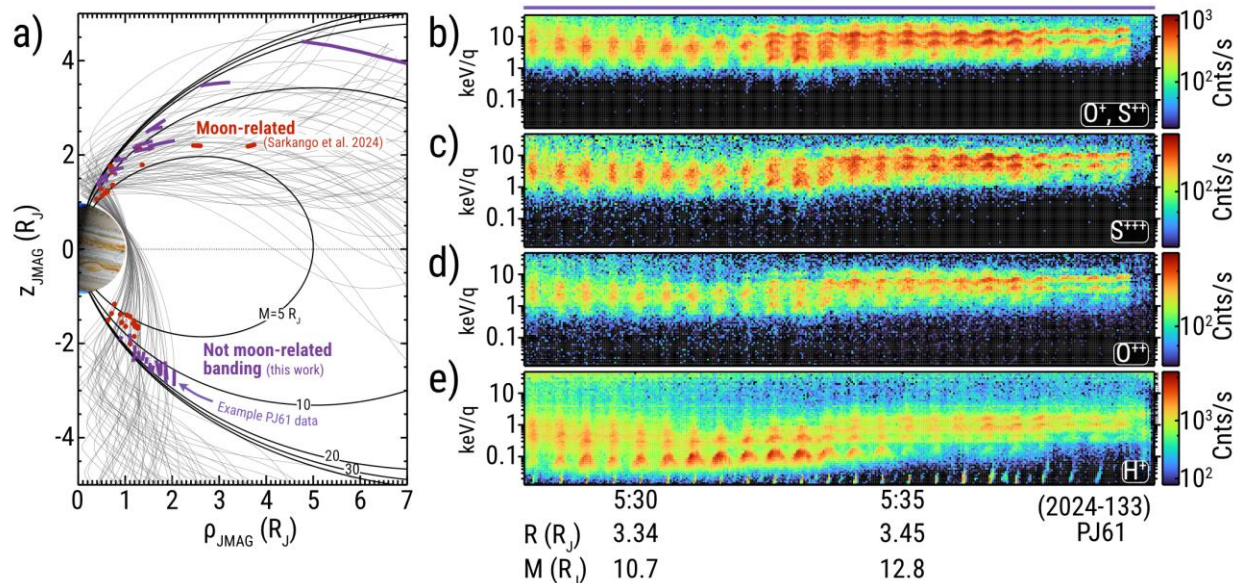


Figure 1. (a) Locations of all possible banded energy distributions observed in the JADE data so far between 2016-2024 in a dipole-centric coordinate system. Moon-related intervals discussed in Sarkango et al. (2024) are highlighted in red. Other intervals with ion banding discussed in the present work are highlighted in purple. (b-e) Energy distributions during the southern pass near perijove 61 (2024, DOY 133) of different ion species (H^+ , O^{++} , S^{+++} , O^+/S^{++}) separated by JADE-I using the TOF measurement.

We analyze one such event in more detail. Figures 1b-1e show the high-rate energy spectra for different mass-per-charge ion species as measured by JADE. These spectrograms are created by converting from TOF \times E to (ion mass in AMU) \times E space using a response function (Kim et al., 2020), then averaging over the count rates in AMU \times E space within a window of $\pm 10\%$ of each m/q value, following previous techniques for generating species-dependent energy-time spectrograms (Szalay et al., 2024). Figures 1b-1e focus on a period of ~ 10 min during PJ 61 (2024, DOY 133). Note that this interval is much longer than those found associated with the moon footprint tail crossings (Sarkango et al., 2024), which lasted for ~ 10 -60 s near the moons' auroral footprints. During this longer interval, *Juno* was transiting across M-shells from approximately $M=10$ to 20, i.e. mapping to larger M-shells with increasing time. Flux enhancements (i.e., bands) were observed for H^+ between ~ 0.1 -2 keV, and for heavier species (O^{++} , S^{+++} , and O^+/S^{++}) between ~ 1 -20 keV. The 30 s intermittency in the bands is due to *Juno*'s spin causing a regular time-varying look direction dependence. This indicates a pitch-angle dependence of the bands because of JADE-I's changing field-of-view. For all ion species, the band at the lowest energies (~ 0.1 keV for H^+) was absent for $M > 13$. The disappearance of lowest-energy bands with increasing M-shell was also seen in the *Cassini* H^+ observations by Thomsen et al., (2017).

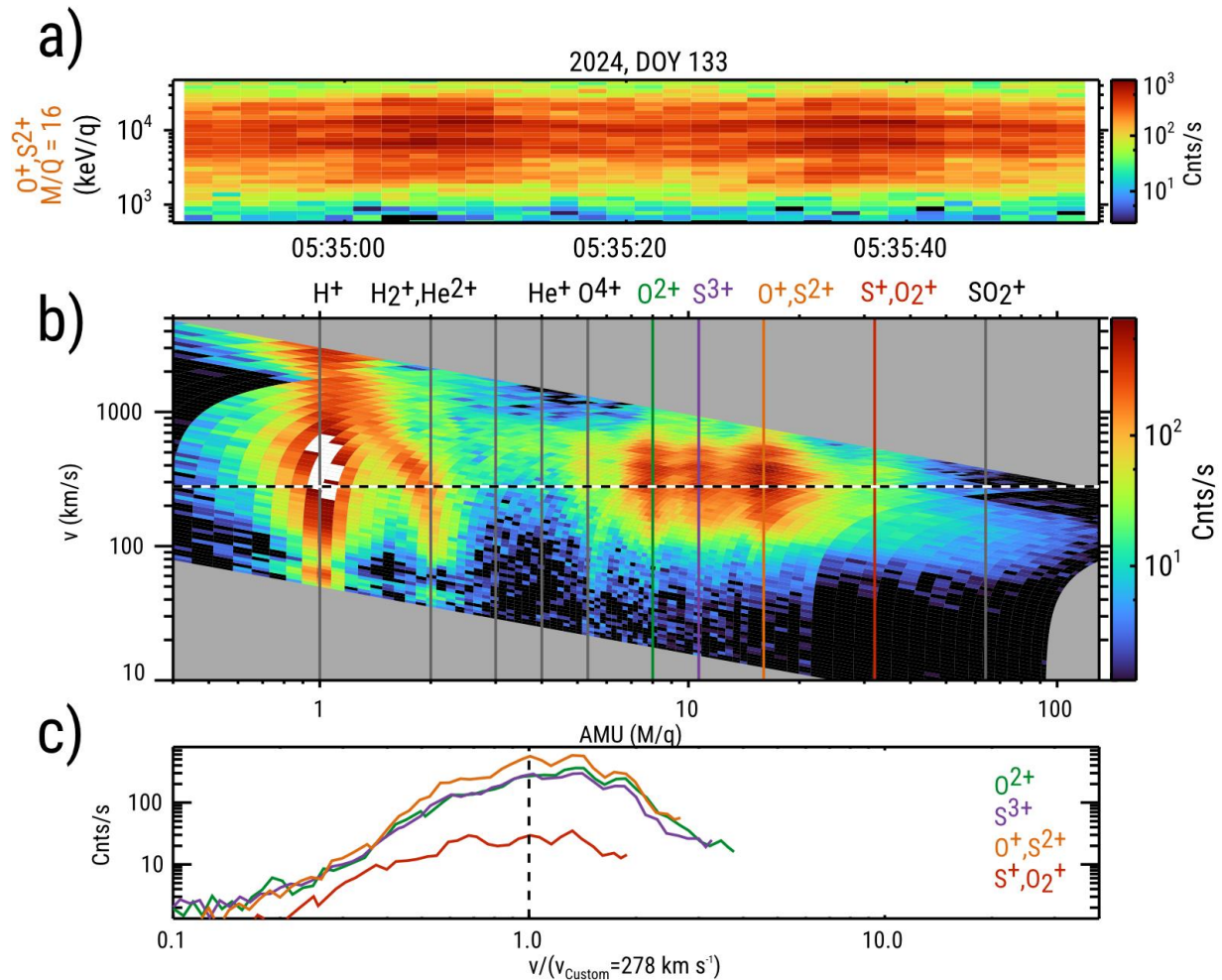


Figure 2. Processed time-of-flight data from JADE-I during the interval shown in Figure 1, showing (a) the energy spectra extracted for $m/q=16$ ions, (b) the count-rate at different measured particle speeds and mass-per-charge (m/q). Different ion species can be identified based on their m/q ratios. (c) Measured count-rate extracted along specific m/q ratios corresponding to the major heavy ion species. Banded flux intensifications are present at nearly the same speeds for all measured heavy ion species. The dashed line is centered on a band at $v = 278 \text{ km s}^{-1}$.

Figure 2 shows a processed JADE-I time-of-flight spectra during the event in Figure 1. Panel a) shows the energy spectra extracted for $m/q=16$, and panel (b) shows the measured count rates with ion mass-per-charge on the X-axis and particle speed on the Y-axis. This representation of the rates demonstrates that although the bands were observed at different energies for different ion species, they occur at the same speeds across all species. This can also be seen visually in Figure 2c, where the count-rate spectrum was extracted along each fixed m/q value.

Since particle bounce periods depend on their speed, these different ion species which exhibit flux enhancements at particular speeds would have the same bounce periods for a given equatorial pitch angle. Since these observations were made at high-latitudes, JADE is sampling only a fraction of the trapped population that have low equatorial pitch angles (typically $< 2^\circ$) and

are able to reach these latitudes. For these small equatorial pitch angles, the bounce periods are more sensitive to energy than the absolute value of the equatorial pitch angle.

We estimate bounce periods by the following expression (Baumjohann & Treumann, 2022),

$$\tau_b = 4 \int_0^{s_m} \frac{ds}{v_{\parallel}} = 4 \int_0^{s_m} \frac{ds}{v \sin \alpha} = \frac{4}{v} \int_0^{s_m} \frac{ds}{\sqrt{1 - \frac{\sin^2 \alpha_{eq}}{B_{eq}} B(s)}} \quad (1)$$

where v is the particle's speed, B_{eq} is the equatorial field strength at a particular M-shell, α is the local pitch angle, α_{eq} is the equatorial pitch angle for the particle, and $B(s)$ is the field strength at a parameterized distance s along the field line. The integration is performed numerically using the dipole approximation of the JRM09 field model in combination with the CON2020 current sheet model. We assume an axisymmetric dipole field because the concept of an M-shell is not really meaningful for a non-axisymmetric field with azimuthal asymmetry. This approximation represents the ‘‘average’’ bounce period across all longitudes. Bounce frequencies in [Hz] are the inverse of the bounce period ($\omega_b = 1/\tau_b$) in [s].

3 Interpretation

3.1. Occurrence of the banded distributions

The banded ions have been frequently observed throughout *Juno*'s tour through the Jovian magnetosphere. There is significantly more organization to when/where these bands are observed in the northern vs. southern hemisphere. *Juno* persistently observed banded ions in the southern hemisphere when it transited radial distances of 2.1-3.5 R_J and M-shells of 9-22 R_J . However, in the northern hemisphere, these features were observed in a more extended region and were less organized in M-shell. Some of this discrepancy may be due to the observational bias and asymmetry in coverage of *Juno*'s orbit between the two hemispheres. Alternatively, this could be a result of a more dipolar southern hemisphere and a highly non-axisymmetric magnetic field in the northern hemisphere that introduces azimuthal asymmetry (Connerney et al., 2018). Yet, the persistent observation of these bands provides evidence that the process of sustaining them is a fundamental process operating continually in Jupiter's magnetosphere.

Banded distributions were observed near the polar regions, mapping to M=10-20. *Juno* has transited through the equatorial regions between the same M-shells, but banded energy distributions were not observed by JADE near the equator. Perhaps this is because bounce periods of particles are dependent on equatorial pitch angle. Near the equator, particles are observed for a range of equatorial pitch angles, and there are many combinations of pitch angles and energies that would be bounce-resonant at some frequency. In contrast, observations made in the polar regions near Jupiter on similar M-shells represent a narrow subset of the trapped population (typically $\alpha_{eq} < 2^\circ$), and the bounce periods for this subset population are more sensitive to particle energy than equatorial pitch angle. Hence, this is one possibility for why flux enhancements in energy, representative of bounce-resonance, are so prominent near the poles. This hypothesis is consistent with the bands observed during PJ 61, which were intermittent at *Juno*'s spin period. Especially

at the band at the lowest energy (Figure 1d), a mini-dispersion with time is clearly visible at the 30-s period, likely due to JADE sampling different pitch-angles during *Juno*'s spin. However, this dispersion does not appear prominent at higher energies. Note that JADE's energy channels are spaced logarithmically, so the bandwidth of the highest energy channels (e.g. at 10 keV) is much larger than the bandwidth of the smaller channels (e.g. at 10 eV), and small dispersions (e.g. at $\Delta E=10$ eV) are hence resolved insufficiently at the highest energies.

It is also worth asking why the banded distributions were only observed between $M=10$ -20. Beyond $M=20$, plasma is not rigidly corotating, and there exists a strong current sheet. The presence of a current sheet could interfere with the bounce motion (Cheng & Decker, 1992; Speiser et al., 2013), although this effect is weaker for lower energy particles whose gyroradii are typically much smaller than the radius of magnetic curvature. We also note that it is unlikely that the observed bands result from instrumental artifacts, since the banded distributions were observed in the same polar regions across many perijove passes and were observed for different ion species at the same speeds.

3.2. Correspondence between bounce-periods and the System-III periodicity

In Figure 3a we use the example from PJ 61-S (from Figure 1) to highlight the different bands in the H^+ spectra. Points were identified for each band by eye and are highlighted in distinct colors in panel (a). Each band has some bandwidth that is most prominently seen in the lowest energy band that ranges from ~ 30 -100 eV. Other bands also have a finite width in energy, but this is difficult to resolve at the higher energy levels, since the bands are resolved in fewer energy channels.

The bounce frequencies for particles depend on the field line geometry and vary with M -shell, in addition to equatorial pitch angle and energy. The corresponding bounce frequencies for each band in Figure 3a, calculated using a JRM09-dipole and CON2020 current-sheet model and assuming a 3° equatorial pitch angle (choosing 1° instead would not particularly change the results) are shown in Figure 3b and they exhibit the linear spacing that is characteristic of bounce resonance. Error-bars are shown for the lowest energy band in red representing the energy bandwidth (identified by eye), but the same is not done for the higher energies as the resolution at higher energies is not sufficient.

Jupiter rotates at the System-III frequency ($\Omega_J = 1/(9.92 \text{ hours}) = 0.028 \text{ mHz}$) (Seidemann & Divine, 1977) and the magnetospheric plasma does not corotate rigidly beyond $M \sim 15$ -20 (Bagenal et al., 2016), so the flow sub-corotation frequency ω_ϕ is smaller than the System-III frequency ($\omega_\phi < \Omega_J$). It can be seen in Figure 3b that bounce frequencies of different bands show good correspondence with integer multiples of the System-III frequency ($\Omega_J, 2\Omega_J, 3\Omega_J, \dots$), shown as horizontal dashed lines. This is indicative of a resonant interaction between the mirroring plasma ions at energies < 10 keV and rigid-corotation with Jupiter, which has not been observed or discussed before in the literature.

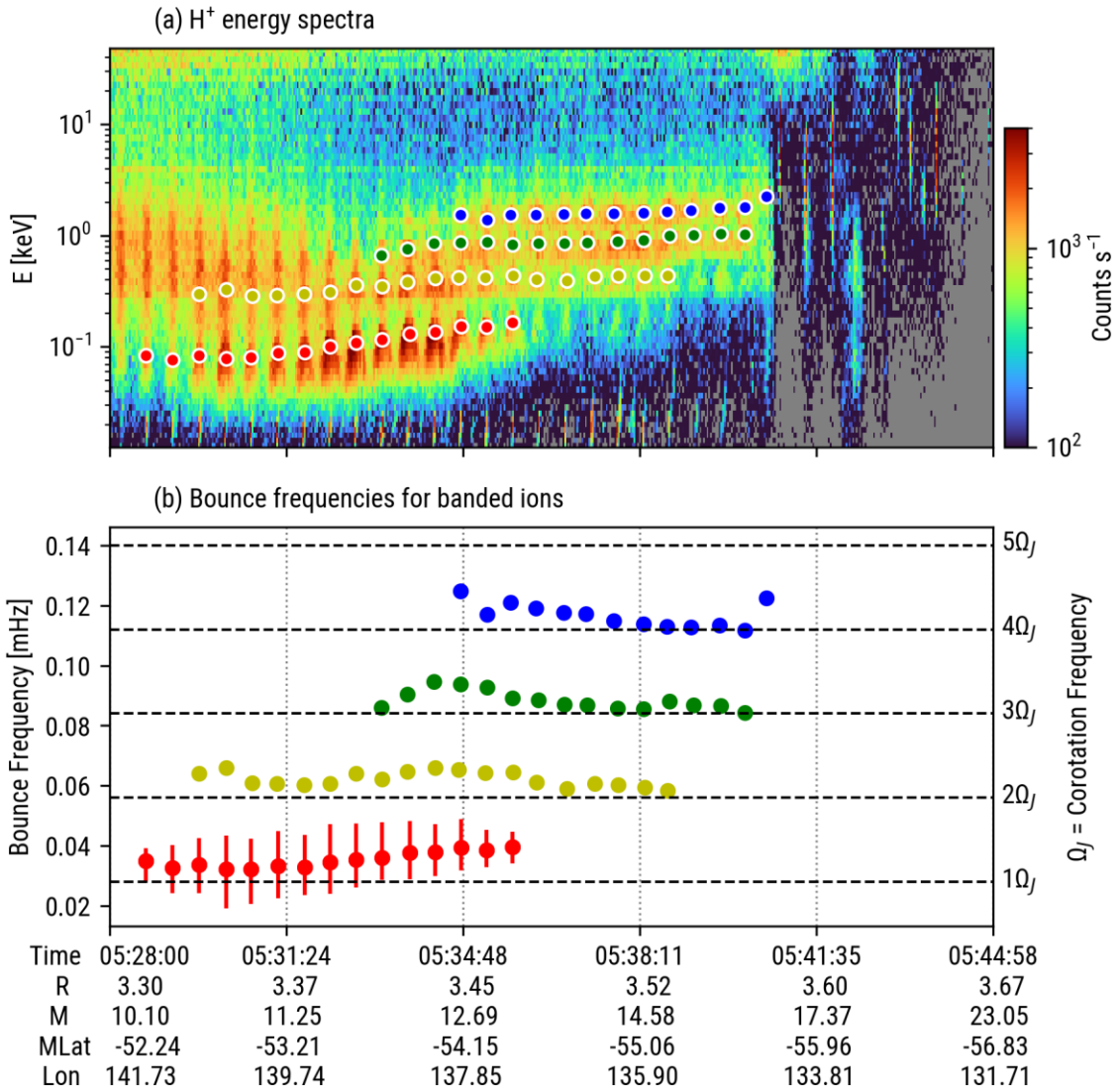


Figure 3. (a) H^+ energy-time spectra during the same interval as in Figure 1 with different bands highlighted in red, yellow, green, and blue points. (b) Bounce frequencies for the banded ions (assuming $\alpha_{eq} = 3^\circ$) compared to integer multiples of the corotation or System-III frequency with respect to Jupiter.

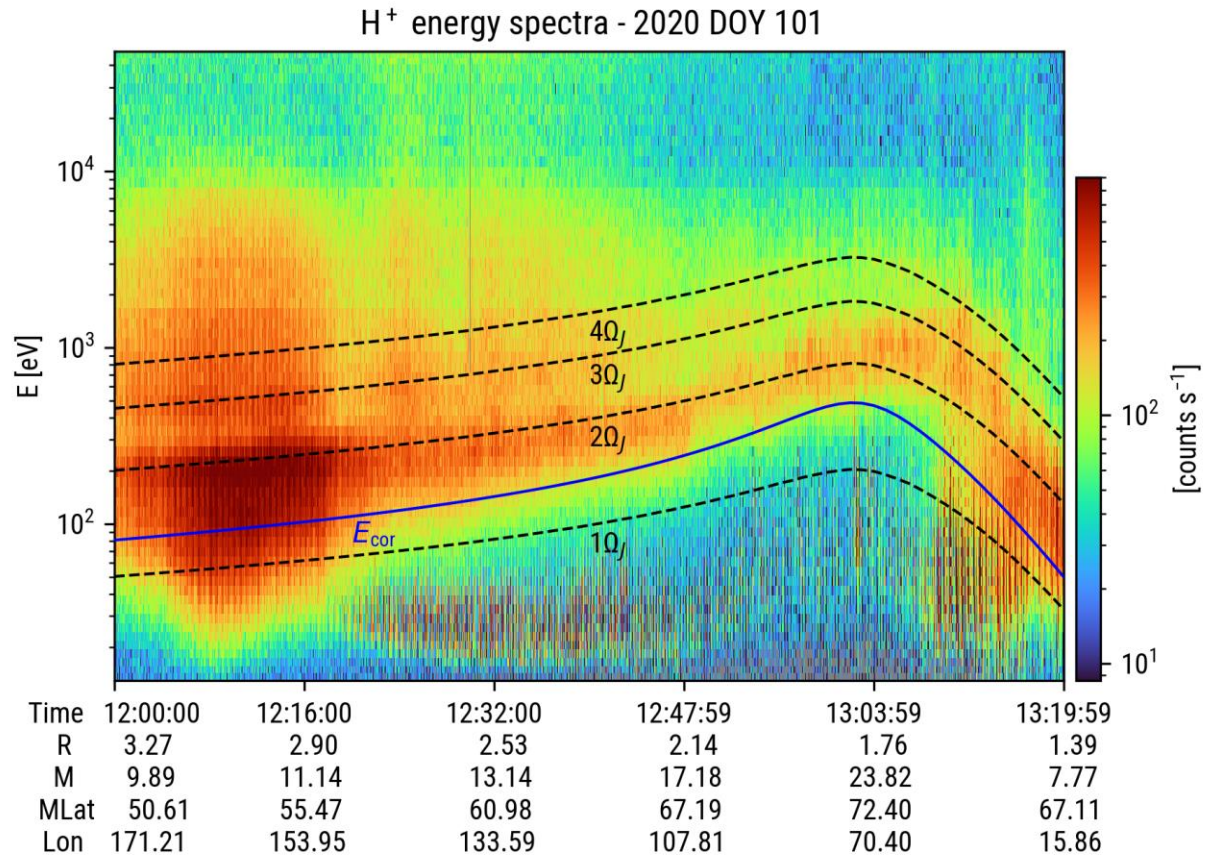


Figure 4. H^+ energy spectra during an interval on 2020, DOY 101 (PJ 26). Except for a singular peak energy with maximum counts, no additional bands were observed during this interval. The blue curve indicates $E_{cor} = \frac{1}{2} m_p v_{cor}^2$, where $\mathbf{v}_{cor} = \boldsymbol{\Omega}_J \times \mathbf{r}_{eq}$, and $r_{eq}(M) = M$, i.e., E_{cor} is the energy associated with proton corotation flow at the equator for some M-shell. Dashed black curves indicate energies at which H^+ ions are expected to be bounce-resonant with the corotation frequency Ω_J .

In Figure 4 we show H^+ energy distributions during an interval between 12:00-13:20 on 2020, DOY 101 (PJ 26) during which no bands were observed, however the count-rate peaks at a certain energy. During this time *Juno* is in the polar regions of Jupiter at an M-shell of $M=9.8$, and transits through magnetic field lines until it reaches a maximum M-shell of $M=24$, and then returns to smaller M-shell values of $M=7.7$. Over this time, the peak-count energy increases until the maximum M-shell value and then decreases.

Assuming a Maxwellian distribution in phase-space that is corotating with Jupiter, the peak phase space density is expected to be at E_{cor} where $E_{cor} = \frac{1}{2} m_p v_{cor}^2$ and $\mathbf{v}_{cor} = \boldsymbol{\Omega}_J \times \mathbf{r}$ (here Ω_J needs to be in units of [rad s⁻¹]), so it is expected that this energy also increases with increasing M-shell. We calculated E_{cor} by identifying *Juno*'s M-shell using the JRM09 internal field and the CON2020 current sheet model (Connerney et al., 2018, 2020). The blue curve in Figure 4 shows the expected E_{cor} at the magnetic equator. The E_{cor} curve follows the energy of the peak-count-rate but differs by a factor of ~ 2 . This could be because the energy with maximum measured

counts differs from the energy with maximum phase space density. This anomaly is discussed in more detail in the Supporting Information.

The energies at which particle bounce frequencies correspond to harmonics of the corotation frequencies, i.e., when $\omega_b = [\Omega_J, 2\Omega_J, 3\Omega_J, \dots]$ Hz, are shown as dashed black lines in Figure 4. In particular, there is close correspondence between peak-count energy and the energy at which $\omega_b = 2\Omega_J$. That is, even in the case when particle distributions are not banded, there appears to be some correspondence between particle bounce motion and the System-III periodicity. The corotation energy $E_{cor} = \frac{1}{2}m_p v_{cor}^2$ (in blue) has a similar trend to these curves, varying with M-shell, but appears to be smaller.

3.3. Hypotheses for corotation-bounce resonance

How would particles that are trapped and bouncing along magnetic field lines experience a resonant interaction with corotation? In particular, resonant wave-interaction requires a modulated electric field in the frame of the particle. We present a few hypotheses for consideration.

1. **Bounce-resonance with Alfvén waves:** Similar to Thomsen et al., (2017)’s Saturn observations, it is possible that the banding results from bounce-resonance within standing Alfvén waves. Eigenperiods for field-line resonances between M=10-20 are on the order of 10-80 min (only the fundamental is larger than 80 min) (Lysak & Song, 2020). Meanwhile, harmonics of the corotation period are at ~ 595 min, 297 min, 198 min, 148 min, 119 min, ..., which coincidentally are also the bounce periods for the low-energy ions within the bands. However, the correspondence between corotation and the bounce frequencies of the banded ions cannot be explained easily. One possibility is that corotation acts as a doppler-shift in the drift-bounce resonance condition. That is, resonance occurs when $\omega - m\Omega_J = N\omega_b$, where Ω_J is the rotation frequency of Jupiter. However, in this model, the Alfvén wave has to be “standing” in the non-rotating frame. It is unclear how this is consistent with the fact that Alfvén waves travel predominantly along magnetic field lines and are frozen-in with the corotating plasma, i.e., the field-lines are also corotating.
2. **Bounce-resonance with a dawn-dusk electric field:** Another way for the particle to perceive an electric field modulation is if it encounters a spatially varying electric field structure during its corotation $\mathbf{E} \times \mathbf{B}$ drift, e.g., the dawn-dusk electric field at Jupiter. A resonant interaction is possible if the bounce frequency of the particle corresponds to the corotation frequency. This situation is analogous to the model of bounce-drift resonance within standing Alfvén waves. The resonance condition is a special case of bounce-drift resonance with $\omega = 0$, i.e., $m\omega_d = N\omega_b$, where ω_d is the frequency at which the particle is drifting azimuthally through the electric field structure ($\omega_d = \Omega_J$ for corotating particles). However, plasma between M=10-20 is more likely sub-corotating (e.g. $\omega_d \sim 0.7\Omega_J$) (Bagenal et al., 2016). The observations appear to be consistent with bounce-resonance with the System-III/rigid-corotation periodicity (Ω_J), not the sub-corotation periodicity.
3. **Bounce-resonance due to explicit time-variability of the background magnetic field:** Jupiter’s magnetodisc wobbles due to the non-axisymmetric magnetic field of Jupiter at the System-III periodicity (Krupp et al., 2004). This periodicity is transmitted to the magnetosphere via Alfvén waves that are associated with a non-zero $\partial\mathbf{B}/\partial t$, i.e., an induced

electric field. In addition to the System-III longitude, the Alfvén travel time from the planet to the magnetosphere also varies with local time (Jenkins et al., 2024). Particles may resonate with this periodic perturbation over their bounce motion.

Alternatively, Hones & Bergeson, (1965) showed that in a tilted-dipole geometry, the $\mathbf{E} \times \mathbf{B}$ drift alone is not sufficient to drive stationary particles to corotation. They proposed that corotation could be achieved nevertheless via Fermi acceleration with the changing background magnetic field. This process could occur in a resonant manner.

4 Summary

Simultaneous banded energy distributions of different ion species in Jupiter’s polar regions mapping to M-shells between roughly M=10-20 were often observed by *Juno*’s JADE instrument. The bands were observed at different energies but similar speed for different ions, hinting at a bounce-resonant interaction. The bounce frequencies of ions at the banded energies corresponded to integer multiples of the System-III rigid-corotation frequency (Ω_J), not the sub-corotating frequency.

We propose three plausible mechanisms to explain these observations –

1. Bounce-resonance with Alfvén waves that are “standing” in the non-rotating frame.
2. Bounce-resonance with a spatially varying electric field that the particles are encountering over their $\mathbf{E} \times \mathbf{B}$ drift motion (e.g., a dawn-dusk electric field at Jupiter).
3. Bounce-resonance with an explicitly time-varying non-axisymmetric (tilted dipole) planetary field.

These novel observations illustrate an unexpected link between bounce motion and plasma corotation at low energies in Jupiter’s magnetosphere, i.e., a corotation-bounce resonance (CBR) that is different from other resonances discussed previously in literature. These distributions have been observed frequently by *Juno* and mapping to the same range of M-shells in the middle magnetosphere, indicating that the physical mechanism that produces these distributions is a fundamental and important process operating in Jupiter’s magnetosphere.

Acknowledgments

We are grateful for the efforts of the *Juno* mission teams, allowing for unique opportunities to study the Jovian magnetosphere. This work was supported by NASA grants NFDAP 80NSSC23K0276 and NFDAP 80NSSC23K0665, and through the *Juno* mission’s JADE instrument science team. J. Saur acknowledges funding from the Deutsche Forschungsgemeinschaft (SA 1772/6-1). Y. S. is grateful to V. Dols and Y. Hao for insightful discussions.

Open Research

All JADE data analyzed in this work is publicly available from the NASA Planetary Data System Plasma Interactions Node and can be found at Allegrini, F. et al., (2024).

References

- Allegrini, F., Wilson, R.J., Ebert, R.W., & Loeffler, C. (2024). JUNO J/SW JOVIAN AURORAL DISTRIBUTION CALIBRATED V1.0 [Data set]. NASA Planetary Data System. <https://doi.org/10.17189/1519715>
- Bagenal, F., Wilson, R. J., Siler, S., Paterson, W. R., & Kurth, W. S. (2016). Survey of Galileo plasma observations in Jupiter's plasma sheet: Galileo Plasma Observations. *Journal of Geophysical Research: Planets*, 121(5), 871–894. <https://doi.org/10.1002/2016JE005009>
- Baumjohann, W., & Treumann, R. A. (2022). *Basic space plasma physics* (Third edition). New Jersey: World Scientific.
- Cheng, A. F., & Decker, R. B. (1992). Nonadiabatic particle motion and corotation lag in the Jovian magnetodisk. *Journal of Geophysical Research: Space Physics*, 97(A2), 1397–1402. <https://doi.org/10.1029/91JA02407>
- Connerney, J. E. P., Kotsiaros, S., Oliverson, R. J., Espley, J. R., Joergensen, J. L., Joergensen, P. S., et al. (2018). A New Model of Jupiter's Magnetic Field From Juno's First Nine Orbits. *Geophysical Research Letters*. <https://doi.org/10.1002/2018GL077312>
- Connerney, J. E. P., Timmins, S., Hecceg, M., & Joergensen, J. L. (2020). A Jovian Magnetodisc Model for the Juno Era. *Journal of Geophysical Research: Space Physics*, 125(10). <https://doi.org/10.1029/2020JA028138>
- Hao, Y.-X., Sun, Y.-X., Roussos, E., Liu, Y., Kollmann, P., Yuan, C.-J., et al. (2020). The Formation of Saturn's and Jupiter's Electron Radiation Belts by Magnetospheric Electric Fields. *The Astrophysical Journal Letters*, 905(1), L10. <https://doi.org/10.3847/2041-8213/abca3f>
- Hones, E. W., & Bergeson, J. E. (1965). Electric field generated by a rotating magnetized sphere. *Journal of Geophysical Research*, 70(19), 4951–4958. <https://doi.org/10.1029/JZ070i019p04951>
- Jenkins, A., Ray, L. C., Fell, T., Badman, S. V., & Lorch, C. T. S. (2024). Revealing the Local Time Structure of the Alfvén Radius and Travel Times in Jupiter's Magnetosphere. *Journal of Geophysical Research: Planets*, 129(10), e2024JE008414. <https://doi.org/10.1029/2024JE008414>
- Kim, T. K., Ebert, R. W., Valek, P. W., Allegrini, F., McComas, D. J., Bagenal, F., et al. (2020). Survey of Ion Properties in Jupiter's Plasma Sheet: Juno JADE-I Observations. *Journal of Geophysical Research: Space Physics*. <https://doi.org/10.1029/2019JA027696>
- Krupp, N., Vytanis, M., Woch, J., Lagg, A., & Krishan, K. (2004). Dynamics of the Jovian Magnetosphere. In *Jupiter: The Planet, Satellites and Magnetosphere*. Cambridge University Press, UK.
- Lejosne, S., & Mozer, F. S. (2020). Inversion of the Energetic Electron “Zebra Stripe” Pattern Present in the Earth's Inner Belt and Slot Region: First Observations and Interpretation. *Geophysical Research Letters*, 47(13), e2020GL088564. <https://doi.org/10.1029/2020GL088564>
- Lejosne, S., Fejer, B. G., Maruyama, N., & Scherliess, L. (2022). Radial Transport of Energetic Electrons as Determined From the “Zebra Stripes” Measured in the Earth's Inner Belt and Slot Region. *Frontiers in Astronomy and Space Sciences*, 9, 823695. <https://doi.org/10.3389/fspas.2022.823695>
- Lysak, R. L., & Song, Y. (2020). Field Line Resonances in Jupiter's Magnetosphere. *Geophysical Research Letters*, 47(18). <https://doi.org/10.1029/2020GL089473>

- Manners, H., & Masters, A. (2019). First Evidence for Multiple-Harmonic Standing Alfvén Waves in Jupiter’s Equatorial Plasma Sheet. *Geophysical Research Letters*, *46*(16), 9344–9351. <https://doi.org/10.1029/2019GL083899>
- Manners, H., Masters, A., & Yates, J. N. (2018). Standing Alfvén Waves in Jupiter’s Magnetosphere as a Source of ~10- to 60-Min Quasiperiodic Pulsations. *Geophysical Research Letters*, *45*(17), 8746–8754. <https://doi.org/10.1029/2018GL078891>
- Pandya, M., Ebihara, Y., Tanaka, T., & Manweiler, J. W. (2023). Formation of Electron Zebra Stripes Observed on 8 September 2017. *Journal of Geophysical Research: Space Physics*, *128*(4), e2022JA030950. <https://doi.org/10.1029/2022JA030950>
- Pandya, M., Ebihara, Y., Tanaka, T., Manweiler, J. W., & Vines, S. K. (2024). Intensification of the Electron Zebra Stripes in the Earth’s Inner Magnetosphere During Geomagnetic Storms. *Geophysical Research Letters*, *51*(3), e2023GL107822. <https://doi.org/10.1029/2023GL107822>
- Roussos, E., Kollmann, P., Krupp, N., Paranicas, C., Dialynas, K., Sergis, N., et al. (2018). Drift-resonant, relativistic electron acceleration at the outer planets: Insights from the response of Saturn’s radiation belts to magnetospheric storms. *Icarus*, *305*, 160–173. <https://doi.org/10.1016/j.icarus.2018.01.016>
- Sarkango, Y., Szalay, J. R., Sulaiman, A. H., Damiano, P. A., McComas, D. J., Rabia, J., et al. (2024). Resonant Plasma Acceleration at Jupiter Driven by Satellite-Magnetosphere Interactions. *Geophysical Research Letters*, *51*(5), e2023GL107431. <https://doi.org/10.1029/2023GL107431>
- Sauvaud, J. -A., Walt, M., Delcourt, D., Benoist, C., Penou, E., Chen, Y., & Russell, C. T. (2013). Inner radiation belt particle acceleration and energy structuring by drift resonance with ULF waves during geomagnetic storms. *Journal of Geophysical Research: Space Physics*, *118*(4), 1723–1736. <https://doi.org/10.1002/jgra.50125>
- Seidelmann, P. K., & Divine, N. (1977). Evaluation of Jupiter longitudes in System III (1965). *Geophysical Research Letters*, *4*(2), 65–68. <https://doi.org/10.1029/GL004i002p00065>
- Speiser, T. W., Dusenbery, P. B., Martin, R. F., & Williams, D. J. (2013). Particle Orbits in Magnetospheric Current Sheets: Accelerated Flows, Neutral Line Signature, and Transitions to Chaos. In G. R. Wilson (Ed.), *Geophysical Monograph Series* (pp. 71–79). Washington, D. C.: American Geophysical Union. <https://doi.org/10.1029/GM062p0071>
- Sun, Y. X., Roussos, E., Hao, Y. X., Zong, Q. -G., Liu, Y., Lejosne, S., et al. (2021). Saturn’s Inner Magnetospheric Convection in the View of Zebra Stripe Patterns in Energetic Electron Spectra. *Journal of Geophysical Research: Space Physics*, *126*(10), e2021JA029600. <https://doi.org/10.1029/2021JA029600>
- Sun, Y. X., Hao, Y. -X., Roussos, E., Zong, Q. -G., Liu, Y., Zhou, X. Z., et al. (2022). Zebra Stripe Patterns in Energetic Ion Spectra at Saturn. *Geophysical Research Letters*, *49*(4), e2021GL097691. <https://doi.org/10.1029/2021GL097691>
- Szalay, J. R., Saur, J., McComas, D. J., Allegrini, F., Bagenal, F., Bolton, S. J., et al. (2024). Europa Modifies Jupiter’s Plasma Sheet. *Geophysical Research Letters*, *51*(6), e2023GL105809. <https://doi.org/10.1029/2023GL105809>
- Thomsen, M. F., Badman, S. V., Jackman, C. M., Jia, X., Kivelson, M. G., & Kurth, W. S. (2017). Energy-banded ions in Saturn’s magnetosphere. *Journal of Geophysical Research: Space Physics*, *122*(5), 5181–5202. <https://doi.org/10.1002/2017JA024147>

- Ukhorskiy, A. Y., Sitnov, M. I., Mitchell, D. G., Takahashi, K., Lanzerotti, L. J., & Mauk, B. H. (2014). Rotationally driven ‘zebra stripes’ in Earth’s inner radiation belt. *Nature*, 507(7492), 338–340. <https://doi.org/10.1038/nature13046>
- Wang, Z., Liu, Y., Zong, Q., Zou, H., Ye, Y., Zhou, X., et al. (2024). Simulations of electron zebra stripes in the inner radiation belt using a composite empirical electric field model. *Science China Earth Sciences*. <https://doi.org/10.1007/s11430-024-1336-8>

Geophysical Research Letters

Supporting Information for

Corotation-bounce resonance of ions in Jupiter's magnetosphere

Y. Sarkango¹, J. R. Szalay¹, P. A. Damiano², A. H. Sulaiman³, P. A. Delamere², J. Saur⁴, D. J. McComas¹, R. W. Ebert^{5,6}, F. Allegrini^{5,6}

¹Department of Astrophysical Sciences, Princeton University, USA

²Geophysical Institute, University of Alaska Fairbanks, USA

³School of Physics and Astronomy, University of Minnesota, USA

⁴Institut für Geophysik und Meteorologie, Universität zu Köln, Germany

⁵Southwest Research Institute, USA

⁶Department of Physics and Astronomy, University of Texas at San Antonio, USA

Corresponding author: Yash Sarkango (sarkango@princeton.edu)

Contents of this file

Table S1. List of non-moon-related banding intervals.

Table S2. List of moon-related banding intervals (Sarkango et al. 2024).

Text S1. Peak count-rate vs. peak phase space density.

Table S1. List of non-moon-related banding intervals.

PJ	Start	Stop
1	2016-240T04:36:41	2016-240T08:17:52
1	2016-240T12:12:06	2016-240T12:15:15
7	2017-191T22:53:54	2017-191T23:16:58
7	2017-192T01:19:10	2017-192T01:20:32
17	2018-355T16:17:15	2018-355T16:32:45
18	2019-043T16:43:42	2019-043T16:49:20
19	2019-096T10:24:06	2019-096T10:44:06
20	2019-149T06:24:46	2019-149T06:35:00
21	2019-202T03:00:50	2019-202T03:07:59
22	2019-255T02:25:58	2019-255T02:28:13
27	2020-154T08:57:32	2020-154T09:10:19
32	2021-052T16:13:46	2021-052T16:26:12
33	2021-105T22:41:16	2021-105T22:44:21
34	2021-159T06:57:57	2021-159T06:59:04
35	2021-202T07:21:51	2021-202T07:26:53
37	2021-289T15:33:47	2021-289T15:53:24
37	2021-289T16:13:45	2021-289T16:18:33
37	2021-289T18:11:47	2021-289T18:19:09
38	2021-333T13:34:27	2021-333T13:45:09
38	2021-333T15:29:31	2021-333T15:34:20
40	2022-056T02:56:49	2022-056T02:59:10
41	2022-099T16:58:26	2022-099T17:05:39
42	2022-143T03:31:08	2022-143T03:37:30
43	2022-186T08:31:31	2022-186T08:33:34
44	2022-229T16:09:47	2022-229T16:14:22
48	2023-022T07:02:58	2023-022T07:08:57
49	2023-060T07:23:34	2023-060T07:29:03
53	2023-212T10:40:54	2023-212T10:50:59
54	2023-250T13:31:35	2023-250T13:36:36
55	2023-288T12:36:01	2023-288T12:47:31
57	2023-364T14:13:04	2023-364T14:28:13
58	2024-034T23:04:37	2024-034T23:09:22
60	2024-100T10:19:34	2024-100T10:33:45
61	2024-133T05:27:19	2024-133T05:39:19
63	2024-198T16:03:33	2024-198T16:12:54

Table S2. List of moon-related banding intervals (Sarkango et al., 2024).

Moon	Start	Stop
Io	2017-086T09:30:51	2017-086T09:31:02
Io	2017-139T06:39:53	2017-139T06:40:04
Io	2017-192T02:22:27	2017-192T02:22:54
Io	2018-144T05:13:11	2018-144T05:13:20
Io	2018-197T04:49:50	2018-197T04:50:12
Io	2018-250T01:46:00	2018-250T01:46:17
Io	2019-043T14:55:50	2019-043T15:02:38
Io	2019-255T03:18:52	2019-255T03:19:07
Io	2019-307T22:07:02	2019-307T22:07:19
Io	2019-307T23:10:38	2019-307T23:10:56
Io	2019-360T18:30:16	2019-360T18:32:24
Io	2020-154T08:26:12	2020-154T08:31:19
Io	2021-052T18:23:13	2021-052T18:23:47
Io	2021-106T00:18:06	2021-106T00:18:43
Io	2021-202T07:10:50	2021-202T07:11:10
Io	2021-245T22:21:57	2021-245T22:22:16
Io	2021-289T17:59:23	2021-289T17:59:56
Io	2021-333T15:10:17	2021-333T15:12:10
Io	2022-056T01:46:10	2022-056T01:46:17
Io	2022-099T16:40:10	2022-099T16:41:52
Io	2022-272T16:36:53	2022-272T16:37:17
Europa	2017-297T16:27:20	2019-297T16:27:50
Europa	2020-154T09:00:15	2020-154T09:00:35
Europa	2021-052T18:31:21	2021-052T18:31:31
Europa	2022-099T16:51:36	2022-099T16:51:50
Europa	2018-250T00:44:50	2018-250T00:45:02
Europa	2018-250T01:50:06	2018-250T01:50:10
Europa	2022-012T09:47:30	2022-012T09:47:58
Ganymede	2021-289T18:19:17	2021-289T18:20:07
Ganymede	2022-099T14:59:16	2022-099T15:00:41

Text S1. Peak count-rate vs. peak phase space density.

The measured count-rate R [count s⁻¹] is related to the phase space density $f(v)$ [s³ m⁻⁶] at some particle speed v ,

$$R \propto v^4 f(v)$$

Eq (S 1)

Hence, the expected speed for peak count-rate (when $\partial R/\partial v = 0$) is not the same as the peak in phase space density when $\partial f/\partial v = 0$. Count-rate is maximum when

$$\frac{\partial R}{\partial E} = \frac{\partial R}{\partial v} \cdot mv = mv \left(4v^3 f + v^4 \frac{\partial f}{\partial v} \right) = 0.$$

I.e. when,

$$4f + v \frac{\partial f}{\partial v} = 0.$$

Eq (S 2)

Assuming a Maxwellian distribution, $f = Ce^{-\frac{(v-v_0)^2}{v_{th}^2}}$, where T is the temperature and v_0 is the bulk speed, and $v_{th} = \sqrt{k_B T/m}$ is the thermal speed, we find that

$$\frac{\partial f}{\partial v} = -\frac{2(v-v_0)}{v_{th}^2} Ce^{-\frac{(v-v_0)^2}{v_{th}^2}} = -\frac{2(v-v_0)}{v_{th}^2} f.$$

Eq (S 3)

Which implies that, for a drifting Maxwellian distribution, f peaks when $v = v_0$. Substituting Equation S3 into Equation S1 leads to a quadratic equation whose roots are at the peak count-rate-speed.

$$4 + v \left[-\frac{2(v-v_0)}{v_{th}^2} \right] = 0$$

$$v^2 - vv_0 - 2v_{th}^2 = 0$$

Hence, if the phase space density peaks at a speed v_0 , the measured count-rate would peak at a different speed v_c , where,

$$v_c = \frac{1}{2} \left(v_0 \pm \sqrt{v_0^2 + 8v_{th}^2} \right).$$

Eq (S 4)

The same expression is also provided in Szalay et al., (2020). In terms of energy, the peak-count-energy is then,

$$E_c = \frac{1}{2} mv_c^2 = \frac{m}{4} \left(v_0^2 + 4v_{th}^2 \pm v_0 \sqrt{v_0^2 + 8v_{th}^2} \right).$$

Or,

$$E_c = \frac{E_0}{2} + mv_{th}^2 \pm \frac{mv_0}{4} \sqrt{v_0^2 + 8v_{th}^2}.$$

Eq (S 5)

Where $E_0 = 1/2(mv_0^2)$ is the energy at which the maximum phase space density is expected. If the temperature is negligible, e.g. for a beam or for cold plasma ($v_{th} \approx 0$),

$$E_c \approx \frac{E_0}{2} \pm \frac{mv_0^2}{4} \approx E_0.$$

That is, for a very cold plasma or beam, the peak in count-rate and the peak in phase space density would occur at the same energy.

For a warm plasma, if the thermal speed is the same as the mean speed, $v_{th} = v_0$, then

$$v_c \approx \frac{1}{2} \left(v_0 + \sqrt{v_0^2 + 8v_0^2} \right) \approx 2v_0, \text{ and}$$

$$E_c = \frac{1}{2} mv_c^2 \approx 4 \left(\frac{1}{2} mv_0^2 \right) \approx 4E_0.$$

In other words, if the temperature of the plasma is 10 eV, and the expected corotation energy ($1/2mv_{cor}^2$) is also 10 eV, then the energy at which a particle detector collects the most counts would be 40 eV. Interpretation of measured count-rate spectra in hot plasmas should account for this.

References

- Sarkango, Y., Szalay, J. R., Sulaiman, A. H., Damiano, P. A., McComas, D. J., Rabia, J., et al. (2024). Resonant Plasma Acceleration at Jupiter Driven by Satellite-Magnetosphere Interactions. *Geophysical Research Letters*, 51(5), e2023GL107431. <https://doi.org/10.1029/2023GL107431>
- Szalay, J. R., Bagenal, F., Allegrini, F., Bonfond, B., Clark, G., Connerney, J. E. P., et al. (2020). Proton Acceleration by Io's Alfvénic Interaction. *Journal of Geophysical Research: Space Physics*, 125(1). <https://doi.org/10.1029/2019JA027314>